E 4 Material Systems for Information Technologies [1]

M. Angst

Peter Grünberg Institut, Jülich Center for Neutron Science, and JARA-FIT

Forschungszentrum Jülich GmbH

Contents

[1] Lecture Notes of the 43rd IFF Spring School "Scattering Methods for Condensed Matter Research: Towards Novel Applications at Future Sources" (Forschungszentrum Jülich, 2012).

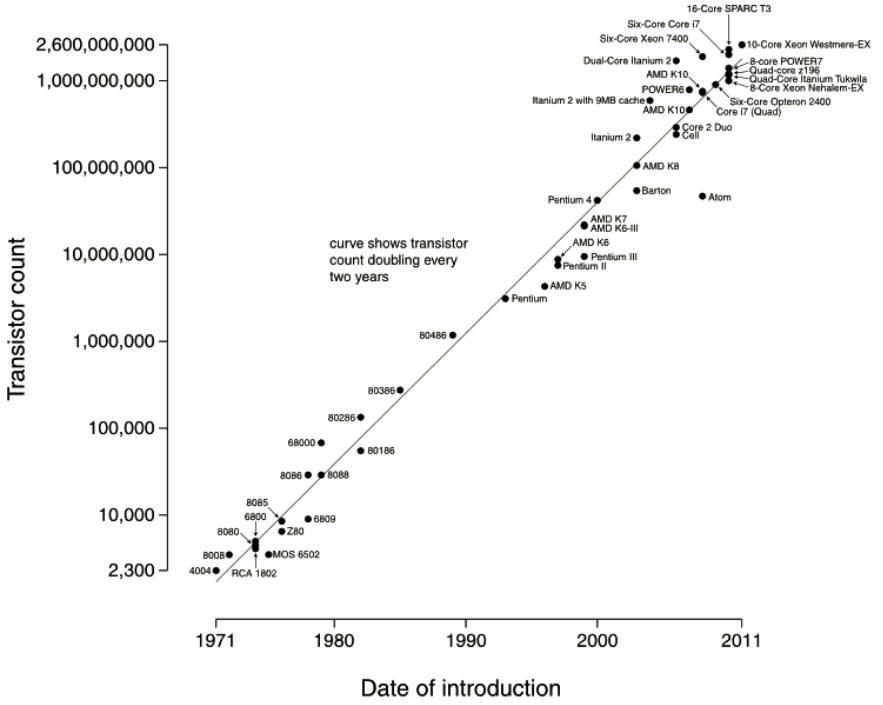

Fig. 1: *"Moore's law" describes the doubling of the number of transistors every two years (Image Source: Wikipedia).*

1 Introduction

Information technology (IT) increasingly permeates all areas of our society and life. It plays a key role in areas as varied as communication and organization, transport and logistics, energy and environmental technology, health and medical care, and last but not least entertainment. The long-term trends in IT are described by Moore's law: the number of transistors placed on integrated circuits doubles every two years (Fig. 1). Similar exponential dependencies also describe computing speed, memory capacity, and, on the downside, costs to build a chip factory and waste heat generated. Although Moore's law has now held for 40 years, it cannot be extrapolated to the future indefinitely. With increasing transistor density implying smaller transistors, about 2025 structures will extend over just a few atoms. This sets a fundamental limit for traditional silicon-based technology: for atomic length scales, quantum effects such as tunneling will hamper device reliability. Furthermore, the waste heat generated by operating these transistors will become unmanageable.

Continuing Moore's law over the next few decades will therefore require fundamentally new concepts and material systems beyond silicon. A large variety of concepts are under investigation, including e.g. quantum computing with quantum dots [1] or superconducting qubits [2], graphene-based transistors [3], redox-based resistive switching [4], spintronics with single-molecular magnets [5], or interfacing with biological systems [6]. Currently it is completely unclear, which of these concepts will succeed in the long run. As it is impossible to cover all of these concepts in more than a superficial way, I will instead focus in this lecture on two concepts, phase change materials and multiferroics, both having a high potential for being applied to vastly improved non-volatile memories already in the near future.

Desirable would be a "universal memory" combining cost benefits of DRAM (used for the main memory of computers), speed of SRAM (used for CPU cache), and non-volatility of flash memory (USB sticks). Furthermore, the ideal memory should have high information density, low power consumption, and a long lifetime (stable over many cycles). Currently the most

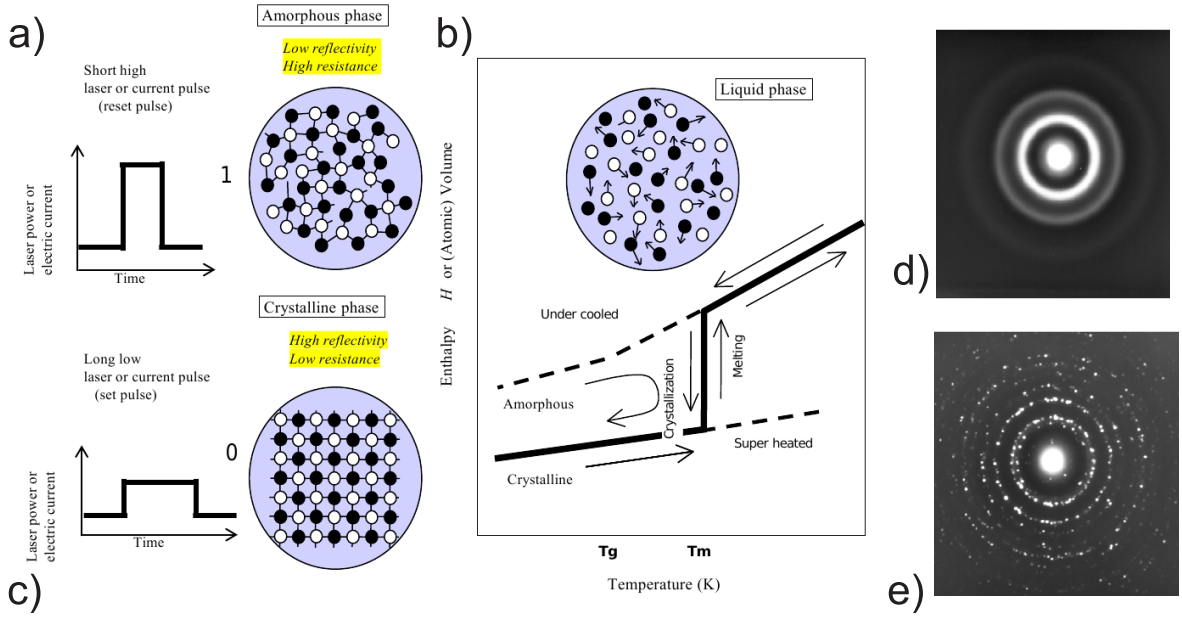

Fig. 2: *a-c) Rewritable optical data storage with PCM (after [7]). a) Short high laser pulse heats the PCM locally, melting it. b) Rapidly cooling quenches the liquid into an amorphous phase with different optical properties from the surrounding crystalline material (detectable by low-intensity laser pulse). c) A long lower-power laser pulse heats the material also to the liquid state, but the less rapid cooling results in crystallization. d/e) Phase contrast between amorphous phase (d) and laser-irradiation-induced polycrystalline state (e) in $Ge_2Sb_2Te_5$ by selected-area electron diffraction (after [8]).*

used non-volatile memory, flash, has high information densities, but a very slow and power-consuming erase operation, and it survives only about 10^5 cycles. Less often used are non-volatile memories based on ferroelectricity, which alleviates some of the drawbacks of flash, but has a low information density. Further, magnetic non-volatile memories (MRAM) are in use, the principle and main drawback of which is addressed in Sec. 3.1.

In the following, first phase change materials (PCM) will be discussed as a route towards an "universal memory" (Sec. 2). After describing the operating principle and the extensive present use of PCM for rewritable optical disks, the main focus is on the unusual structure and bonding underlying the functionality. Next, multiferroics will be considered (Sec. 3). After introducing the concept and the operation principle, the main focus will be on the problem of the incompatibility between traditional ferroelectricity and magnetism, and various mechanisms providing a way around it. The lecture will conclude with a comparison of the application prospects of PCM and multiferroics and a brief discussion of the relevance of scattering methods in elaborating these materials.

2 Phase Change Materials (PCM)

2.1 Rewritable disks and non-volatile memories with PCM

Phase-change materials (PCM) are materials with metastable amorphous and crystalline phases, and fast transformations between them. They are already used in IT, in rewritable optical data

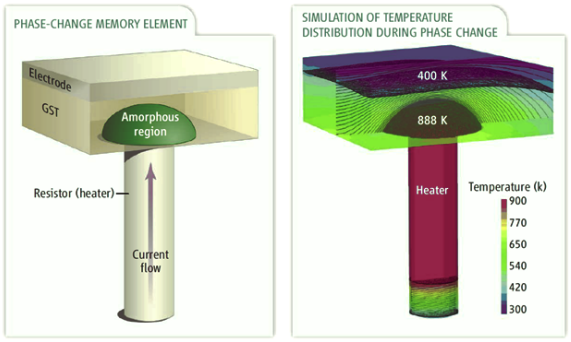

Fig. 3: *Concept of nonvolatile phase-change memory cell. Sketch of the cell and resistive heating to write/erase (left) and simulation of temperature-distribution during phase change. After [11].*

storage media such as newer generations of rewritable DVDs (digital versatile disks) and Blu-ray disks. For such media, the bits are encoded as sections of the PCM in either a crystalline (0) or an amorphous (1) state, both of which have a thermal stability of several decades at room-temperature. For PCM used in optical data storage, considerable differences in the atomic arrangement between amorphous and crystalline phases results in a significant optical contrast. The state of the bit can then be read out by a very low-power laser pulse.

The operating principle of PCM is illustrated in Fig. 2a-c). To write a bit, a short high laser pulse is applied, which heats the material above its melting temperature. Because the melting temperature T_m is far above ambient temperature, the PCM cools very rapidly below the glass forming temperature T_g after the pulse, at rates $\sim 10^9\,\mathrm{Ks}^{-1}$. This leads to quenching of the liquid state into a disordered, amorphous phase. The reverse operation also utilizes heating by a laser pulse, but one that is of lower power over a longer duration, heating the PCM to $T_g \ll T < T_m$. The long pulse duration giving sufficient time for crystallization of the PCM. The phase transformation from amorphous to crystalline by laser irradiation is directly verifiable e.g. by selected-area electron diffraction, see Fig. 2d/e) [8].

For the application several requirements need to be fulfilled: In addition to the long thermal stability of both states at room temperature and to the large optical contrast, suitable materials must be glass formers, but marginal ones, so that both phases can be reached easily. This means typically reduced glass temperatures T_g/T_m between 0.5 and 0.55 [9]: For smaller T_g/T_m it becomes difficult to reliably quench the PCM rapidly enough to reach the amorphous state. For higher T_g/T_m, on the other hand, the crystallization rate is too slow for the material to be of practical use. Additional requirements include a good reversibility of the transition, i.e. a large number of cycles without degradation, and a high chemical stability [7]. Successful examples of PCM include Te-based multicomponent alloys along the GeTe-Sb_2Te_3 quasi-binary tie-line, such as $Ge_2Sb_2Te_5$ [10].

Optical data storage is not the only possible IT application of PCM. Indeed, PCM show also great promise for future non-volatile memory-cells [11]. The operating principle in this case is very similar to the one for optical disks, with the optical contrast between the phases replaced by different (low-current) resistivities and the laser pulse heating replaced by current pulse heating (Fig. 2a-c). The current pulse is applied to a resistive heater placed next to the PCM-region of the cell, as indicated in Fig. 3.

Because strong resistive contrasts are much easier to reach than significant optical contrasts, there could be many more candidate PCMs for non-volatile memory cells than for rewritable optical storage media. In this context I would like to note that historically, resistive switching was how PCM were discovered several decades ago [12], while their use for optical disks was noted only much later.

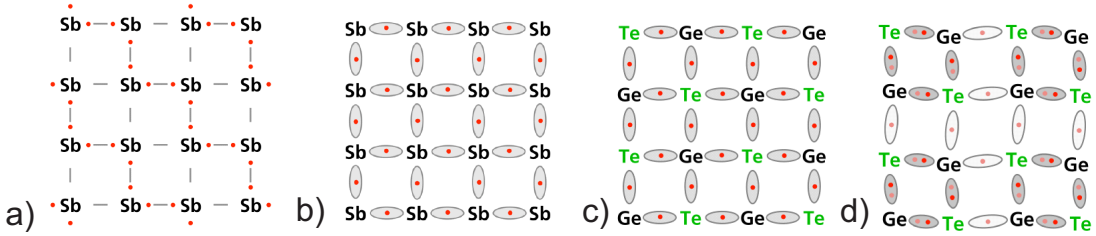

Fig. 4: *Resonant bonding and distortions in Sb and GeTe (2D-projection). a) With covalent p-bonding in Sb, only half of the bonds are occupied. b) Sb resonant bonding with delocalization of the electrons in the bonds. c) Resonant bonding in GeTe. d) as c), but with additional slight distortion. After [14].*

However, the usability for non-volatile memories involves some requirements beyond those for the optical disks. First, the speed of the write and also the erase operations is even more crucial. This implies for example very fast crystallization dynamics, as this is the speed-limiting factor. Crystallization of the order of $100\,\mathrm{ns}$ has been achieved so far [11], which is already two orders of magnitudes better than a cycle in a flash memory. A long lifetime (large number of cycles) is another requirement, which is already orders of magnitude better. Ion migration under the influence of the electric field during switching is the major factor preventing even longer lifetimes [13].
Crucial for operation is also a minimization of waste heat, i.e. the switching should not require unduly high power. Resistivity in the crystalline phase are typically Ohmic and intermediate, which ideally facilitates resistive heating. However, in the amorphous phase the resistivity is extremely high, preventing enough current to flow for the necessary heat to be delivered. Fortunately, at moderate voltages ($< 1\,\mathrm{V}$ for typical dimensions, threshold switching occurs in the amorphous phase [9]: a fast electronic transition into state with much lower resistance. The subsequent current flow then generates the required heat.

2.2 Structure and Bonding

Because the phase change is a structural change there must be a strong relationship between the PCM functionality and the structures of both the crystalline and the amorphous phases. Thus, the structure is examined here, starting with the crystalline phase. For e.g. $Ge_2Sb_2Te_5$ the thermodynamically stable crystal structure is trigonal, but the phase involved in phase change is exclusively a metastable cubic phase (as indicated by diffraction such as the pattern shown in Fig. 2d). This cubic phase corresponds to a slightly distorted NaCl-structure, with the Cl-positions occupied by Te and the Na-positions randomly by Ge, Sb, and vacancies. Thus all the atoms have octahedral (6-fold) coordination. This octahedral coordination is typical for PCM in the crystalline state, but in general highly unusual, as it violates the so-called "$8 - N$ rule" that states that the coordination of an atom in a covalent bonding environment should be $8 - N$ when N is the number of valence electrons. Thus, Ge should be 4-fold coordinated (as is the case for elemental Ge), Sb 3-fold and Te 2-fold.
Consider Sb, also a PCM, in the ideal NaCl-structure. Sb has a $5s^2 5p^3$ valence shell configuration. The $90°$ bond angles for the NaCl structure suggest the absence of $s - p$ hybridization, i.e. only the p-orbitals take part in bonding. With normal covalent bonding only half of the possible bonds are occupied, e.g. those shown in Fig. 4a), or completely equivalently all those

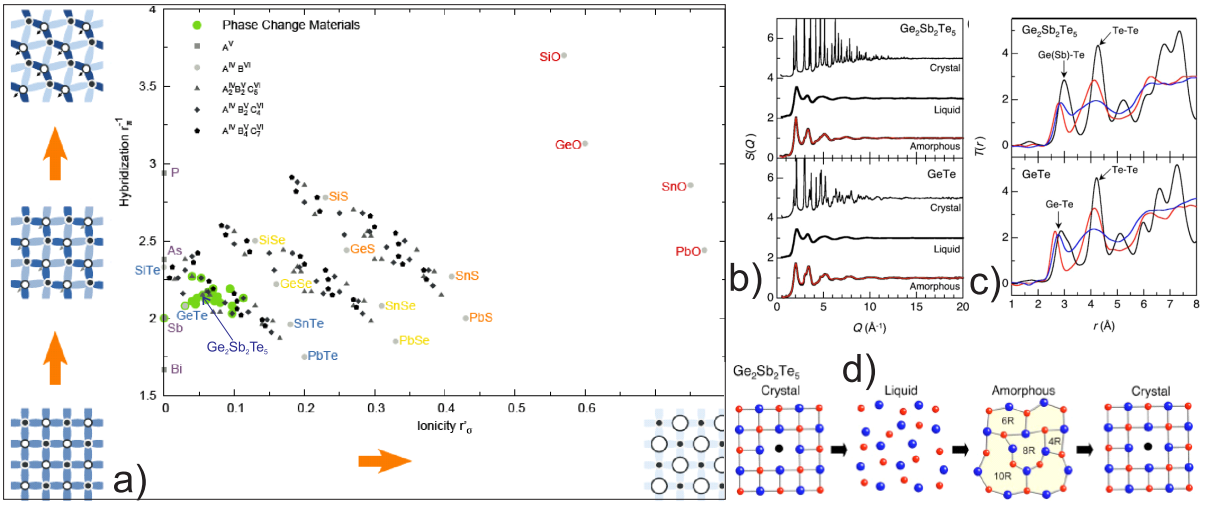

Fig. 5: *a) Treasure map for PCM (after [16]): The x-axis is the ionicity, the y-axis the tendency towards hybridization. PCM are found in a small region of the map that is prone to resonant bonding. b)-d) Local structure of $Ge_2Sb_2Te_5$ and GeTe phases (after [17]). b) total structure factors. c) pair correlation functions for crystal (black), liquid (blue), and amorphous (red) phases. d) Schematic representation of possible ring-size transformation in recording and erasing processes ($Ge_2Sb_2Te_5$).*

not occupied in Fig. 4a). In this situation, a superposition of the two bonding pattern occurs, with highly delocalized electrons (Fig. 4b). This is called resonant bonding [15] and occurs more prominently in benzene. For PCM like GeTe, the picture is analogous (Fig. 4c). Alternatively to resonant bonding, a Peierls distortion can occur, involving alternating short and long bonds, deviation of the angles from $90°$, and the opening of a gap. For large distortions, resonant bonding is no longer possible. But for small distortions (sketched for GeTe in Fig. 4d) as typically occur in the crystalline phase of PCM, the electron localization into half of the bonds is incomplete, and resonant bonding is only weakened. The resonant bonding, even weakened, leads to a high electronic polarizability and low resistivity and is thus the origin of the property contrast in PCM as the transition to the amorphous phase involves a much more distorted state (see below) destroying resonant bonding [14].

To pinpoint the occurrence of resonant bonding, Lencer and coworkers [16] considered a 2D map of materials (Fig. 5a). One coordinate axis is the degree of ionicity of the bonding, which can be parametrized as $r'_\sigma = r_p^{\mathrm{A}} - r_p^{\mathrm{B}}$, where r_p^{A} and r_p^{B} denote the averaged valence radius of the p-Orbital for cations and anions, respectively. The other axis gives the tendency towards $s-p$ hybridization, parametrized as $r_\pi^{-1} = [(r_p^{\mathrm{A}} - r_s^{\mathrm{A}}) + (r_\pi^{-1} = [(r_p^{\mathrm{B}} - r_s^{\mathrm{B}})]^{-1}$, with s denoting the s-orbitals. For high values of r_π^{-1} $s-p$ hybridization becomes inreasingly favorable, resulting in a deviation from octahedral connectivity and coordination number following the $8-N$ rule (see sketches at the left). This excludes resonant bonding. Similarly, increasing ionicity localizes the electrons at the anions (see bottom sketches), also opposing resonant bonding. We thus expect PCM only in the lower left corner of Fig. 5a), which is indeed the case (green dots). This confirms the high relevance of resonant bonding and also provides a tool in the search of further PCM. Whereas the PCM-region is at minimal ionicity, it includes a small but non-zero amount of hybridization tendency. Therefore, while resonant bonding must prevail, it also has to be imperfect, with some propensity towards hybridization.

To understand the strong property contrast between crystalline and amorphous phases despite

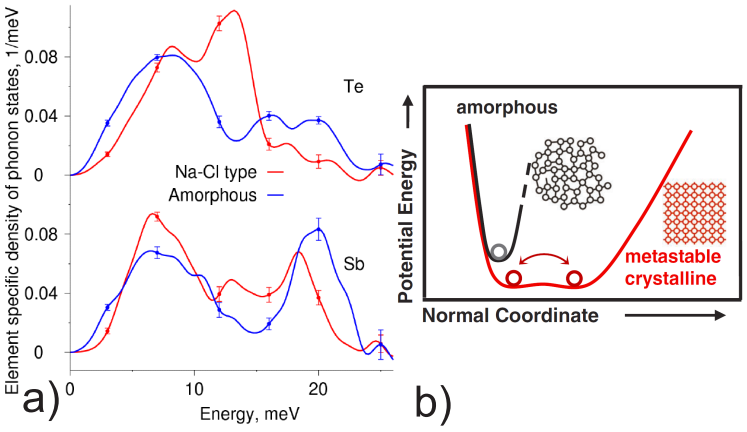

Fig. 6: *a) Elastic hardening and vibrational softening of optical modes: Crystalline (red) and amorphous (blue) $GeSb_2Te_4$ element-specific phonon density-of-states from nuclear-inelastic scattering at* 25 K. *b) Schematic interaction potential for the amorphous (black) and crystalline (red) state of a PCM. After [19].*

of the fast transformations between them, it is also necessary to elucidate the local structure in the amorphous phase. This can be done by total scattering or pair-distribution-function analysis (see lecture D5) or by x-ray absorption spectroscopies (see lecture F4). An example of the application of the former to $Ge_2Sb_2Te_5$ and GeTe is shown in Fig. 5b)-d) [17]: the radial total structure factor of crystal, liquid, and amorphous, phases obtained by x-ray scattering (panel b) by fouriertransform yields the radial pair-correlation functions $T(r)$ (probability to find a second atom at distance r), see panel c). Compared to the crystalline phase (black), $T(r)$ of the amorphous phase (red) is washed out particularly at large r, as expected. However, unusually, there are also pronounced shifts of the peaks indicating the nearest-neighbor distances from Ge(Sb) to Te. Performing Reverse Monte Carlo on the data, Kohara and coworkers obtained the short and intermediate range structure in all $Ge_2Sb_2Te_5$ phases (Fig. 5d). The average coordination numbers for Ge (3.7), Sb (3.0), and Te (2.7) are much closer to the expectation from the $8 - N$ rule than for the crystalline phase, suggesting essentially covalent bonding with $s - p$ hybridization. Despite of these coordination numbers, the bond angle distribution (not shown) peaks at $90°$, indicating a preferentially octahedral environment of the atoms, even if highly defective and distorted. The structure can be described by statistics on ring sizes, with each ring showing pronounced cation-anion alternation (as in the crystalline cubic phase). To a first approximation, the amorphous structure can thus be treated as a highly distorted copy of the cubic phase, but the strong distortion removes the resonant character of the bonding, resulting in the property contrast. Molecular dynamics simulations [18], simulating a whole phase-change cycle, indicate that there is a very high density of 4-rings in the amorphous phase, involving more than 50% of the atoms. These serve as crystallization centers, facilitating the fast transformation to the cubic phase, for which little medium-ranged diffusion is necessary.

2.3 Vibrational properties

Particularly for applications in non-volatile memories, a low thermal conductivity is also important, because it decreases the power necessary to thermally cycle a memory cell. Low thermal conductivities in amorphous phases is typical, but in contrast to most materials, PCM have thermal conductivities in their crystalline phase that is not much higher than in the amorphous phase. This points to unique vibrational properties of the crystalline phases of PCM. These can be assessed e.g. by nuclear inelastic scattering (see lecture D9) yielding the element-specific phonon density-of-state, shown for both phases of the PCM $GeSb_2Te_4$ in Fig. 6a) [19]. Surprisingly, crystallization involves both a hardening of the low-energy acoustic phonons (and

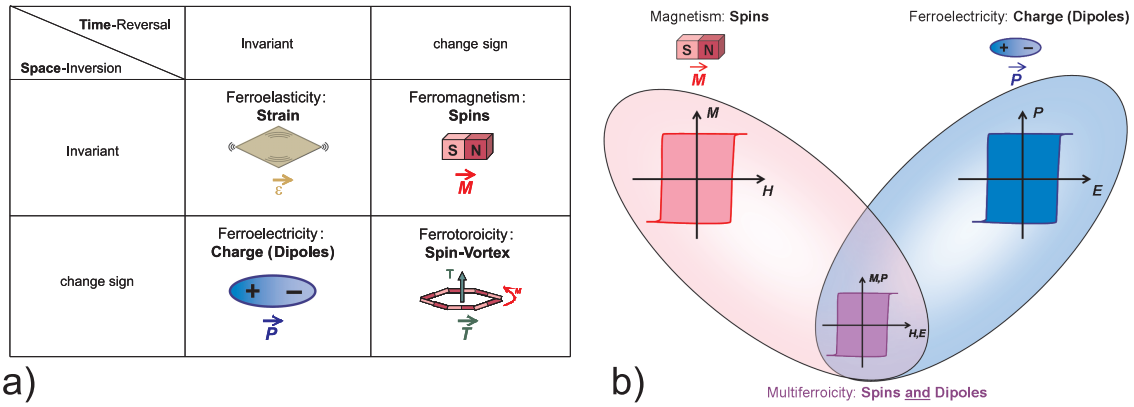

Fig. 7: *a) Classification of "ferroic" orders according to symmetry. b) "Ferroic" also requires coupling of the order parameter to an appropriate field, e.g.* $M(H)$ *or* $P(E)$*, without which the order is termed "antiferroic". "Multiferroics" as a term was coined to label materials combining two or more ferroic orders. In particular, magnetoelectric Multiferroics combine ferromagnetic (FM) and ferroelectric (FE) orders, and the both order parameters may couple to both magnetic and electric fields.*

thus a larger bulk modulus) and a softening of the high-energy optical phonons. The hardening of acoustic phonons corresponds to an increase of the acoustic-mode Debye temperature θ, but only a moderate ($\sim 20\%$) one. The unusual simultaneous softening of the optical phonon modes is an effect of the resonant bonding in the crystalline phase [19]. Because some of the optical phonons are closely related to the tendency towards a Peierls-distortion, this softening suggests a small barrier between the undistorted cubic structure and a Peierls-distorted structure. The interaction potential in the crystalline phase looks thus qualitatively as sketched in Fig. 6b) in red: it is weaker and much more anharmonic than the corresponding potential in the amorphous phase. Consequences of this interaction potential include significant static distortions (observed in form of large displacement parameters) and large thermal expansion (as also observed). Furthermore, the anharmonicity, quantified as the high-T limit of the Grüneisen-Parameter γ, in inversely proportional to the thermal conductivity $\kappa \propto \theta^3\gamma^{-2}$, and thus contributes to the anomalously low thermal conductivity in the crystalline phase. Because the unusual interaction potential arises from the combination of resonant bonding and static distortions, the PCM-region in the treasure map (Fig. 5a) with its low, but not too low propensity towards hybridization, is also the region of solids with low Debye temperatures, anharmonic interactions, and low thermal conductivities, i.e. PCM fulfill this requirement automatically.

3 Multiferroics

3.1 Multiferroics for non-volatile memories

The term "multiferroic" (MF) was coined [20] to describe materials simultaneously exhibiting at least two kinds of ferroic orders. A ferroic order is described as a spontaneous order that can exhibit domains (where the order parameter has different sign or direction), and whose order parameter couples to a suitable external field. For example, in a ferromagnet (FM) the Magnetization (order parameter) can form domains, and it can be switched by (couples to) a magnetic field, represented by a hysteresis loop as sketched in red in Fig. 7b). Ferroic orders can be

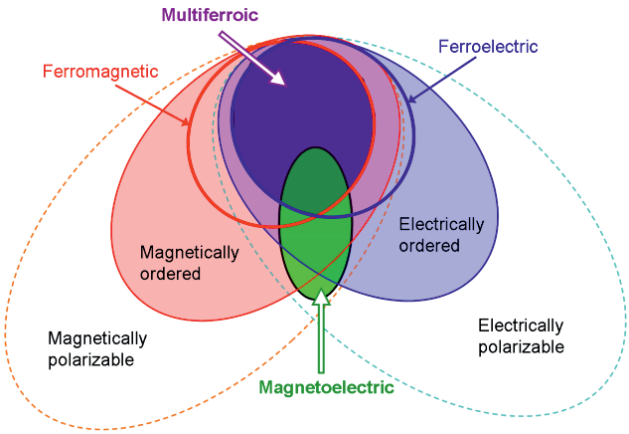

Fig. 8: *Often the term "multiferroic" is used in a wider sense to encompass simultaneously magnetically and electrically ordered materials, e.g. antiferroelectric antiferromagnets. A magnetoelectric coupling can exist within the even wider class of both magnetically and electrically polarizable materials.*

classified according to the transformation-properties of the order parameter upon time-reversal and space-inversion (Fig. 7a). For example, ferroelastic order is invariant under both operations, whereas the order parameter of ferrotoroidicity (the alignment of toroidal moments arising from a ring-like arrangement of spins, see [21] and Fig. 7a) changes sign upon either operation. A ferroelectric (FE) that is also a ferromagnet (magnetoelectric MF) breaks both time-reversal and spatial-inversion symmetries, similar as a ferrotoroidic. The latter are also interesting for magnetoelectric applications, as they intrinsically exhibit a magnetoelectric effect. Research on ferrotoroids is relatively new, and this fascinating topic cannot be covered in detail here, see [21] for a comprehensive review. Despite being relevant for applications, we also omit ferroelastics from further consideration, focusing entirely on magnetoelectrics from now on, writing just multiferroic or MF for magnetoelectric multiferroic.

The combination of FM and FE into a multiferroic is sketched in Fig. 7b). By definition then, such a material has a spontaneous magnetization that is switchable by a magnetic field and a spontaneous electric polarization that is switchable by an electric field. With a sufficient electromagnetic coupling (which is not guaranteed), it is possible that the spontaneous magnetization can also be switched by an electric field, or the polarization by a magnetic field. However, multiferroicity does *not* imply that there is a magnetoelectric effect , and conversely magnetoelectric effects can occur in the much wider class of materials that are simultaneously magnetically and electrically polarizable (Fig. 8). In practice, magnetic and electric ordering tendencies will make a strong magnetoelectric coupling much more likely, however, as indicated above. Since actual FM FE are more rare than antiferromagnetic (AFM) FE, most practitioners have come to use the term "multiferroic" in a wider sense, i.e. designating any magnetically ordered FE (or even including anti-ferroelectric magnetic materials as well). We will follow this convention through the rest of this section.

As mentioned in Sec. 1, multiferroics may also be used for non-volatile memories. Consider the MRAM or magnetic random access memory, a non-volatile memory already in use. Schematically, the already existing MRAM cells look similar to the device depicted in Fig. 9: Information is encoded in the relative direction of the magnetization of two layers (parallel: 0, antiparallel: 1), and it is read out with the giant magnetoresistance (GMR) effect, discovered in 1988 (P. Grünberg, Forschungszentrum Jülich, and A. Fert, U Paris-Sud 11, Physics Nobel Price 2007). The main problem of the MRAM is the write operation requiring remagnetizing a layer with significant currents, making it slow and in particular highly power consumptive. If a layer of an insulating material that converts a voltage to a magnetization could be attached, writing the device could occur with the simple and non-dissipative application of a voltage. The resulting

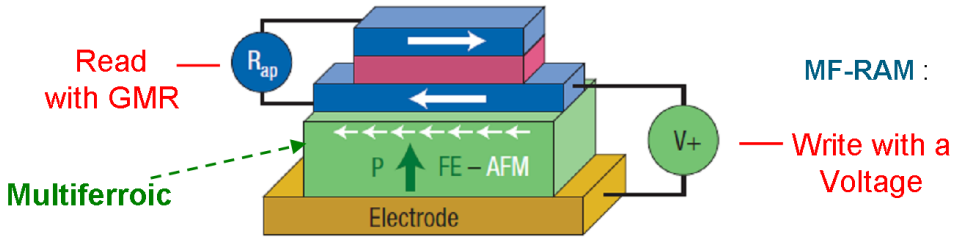

Fig. 9: *Concept of multiferroic memory cell [22]. As in the already existing magnetic RAM (MRAM), the information is encoded in the parallel or antiparallel alignment of the magetization of two layers, read out with the giant magneto-resistance effect. The addition of a layer of magnetoelectrically active (e.g. multiferroic) material allows to write the information by applying a voltage, overcoming the main drawback of MRAM cells.*

cell might be called "multiferroic" RAM or MF-RAM. The principal challenge in realizing the MF-RAM concept is to find a suitable material, for which a magnetoelectric coupling as described above occurs at room temperature and it is strong enough. Luckily, in order to switch the magnetization it is not necessary to have a spontaneous magnetization in the magnetoelectrically active (green in Fig. 9) layer. This is because of a directional magnetic coupling at the interface between adjacent FM and AFM layers that is known as exchange bias (reviewed in [23]). Due to the directionality the magnetization direction in the ferromagnetic layer may follow the direction of the AFM order parameter in the AFM layer. Bi-stable switching of magnetization by an electric field has indeed been demonstrated using exchange-bias and an AFM FE (see Sec. 3.5). However, although AFM instead of FE works, identifying suitable materials is still a challenge.

3.2 Incompatibility between Ferroelectricity and Magnetism and ways around

There are a lot of FM materials as well as a lot of FE ones. However, there are surprisingly few that are both, and understanding why is the first issue to be addressed [24]. One reason for the scarcity of multiferroics is simply symmetry: due to the need of breaking both time-reversal and spatial-inversion symmetries, out of the 122 magnetic point groups there are only 13 that allow for both spontaneous magnetization and electric polarization to occur. Yet, many materials occur in one of these 13 point groups without being multiferroic. A simple reason for the rarity of multiferroics in the strict sense (FM FE) is that ferromagnets tend to be metals whereas sustaining an electric polarization requires a material to be insulating. More interesting is to examine the wider class of magnetic FE, examples of which still turn out to be very rare.
To address this latter question, we focus on perovskite-type ternary oxides ABO_3 with A and B transition metals, which contain both numerous (hundreds) FE and magnetic materials. At high temperatures perovskites have an often slightly distorted, but centrosymmetric, cubic structure. The typical, and "traditional", mechanism of ferroelectricity in these materials is an off-center displacement of the B-site ion (for example Ti in $BaTiO_3$), sketched in Fig. 10a). With a $4+$ valence from electron counting, Ti has an empty d shell. In fact, most FE perovskites have a B ion with empty d shell. Since magnetism requires unpaired d electrons, this automatically prevents multiferroicity in these cases.
Since electrostatic interactions (Coulomb-repulsion between electron clouds on adjacent ions)

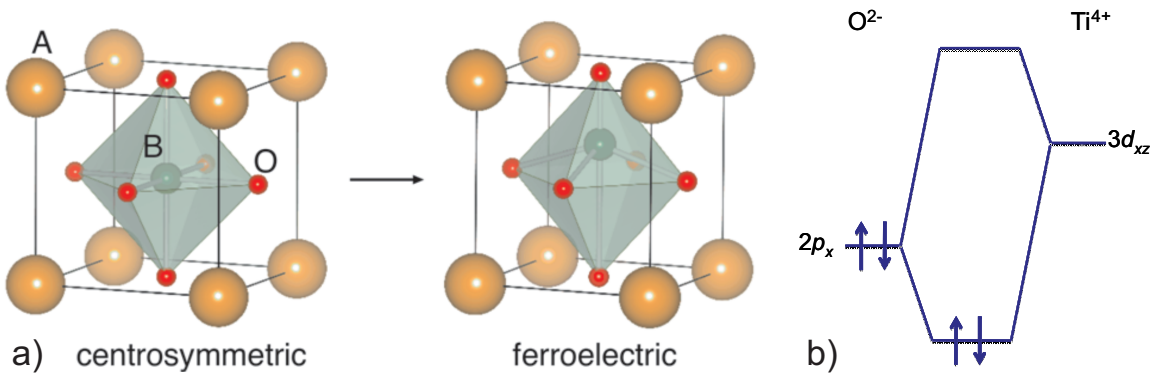

Fig. 10: *"Traditional mechanism of ferroelectricity": a) In perovskites ABO_3 such as $BaTiO_3$, an off-center displacement of the B ion leads to ferroelectricity. b) B-O Hybridisation energy level scheme. If B has an empty d-shell, the shared electrons occupy exactly the bonding state (arrows). Additional electrons from the B d-shells would go into anti-bonding orbitals, lowering any energy gain from hybridisation.*

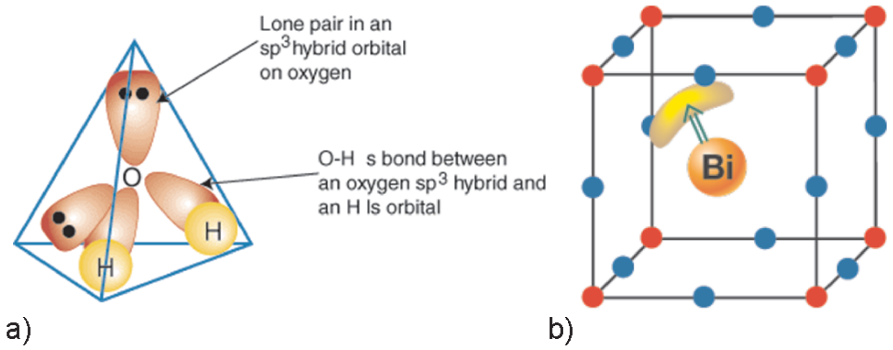

Fig. 11: *a) Oxygen lone pairs in a water molecule. b) Bismuth lone pair in $BiCrO_3$ [27]. The lone pair, if localized, breaks inversion symmetry and can lead to ferroelectricity.*

favor the centrosymmetric arrangement of ions, the B ion displacement must be due to other bonding considerations [24, 25]. Indeed, energy may be gained by formation of strong covalent bonds with one (or three) of the surrounding oxygen ions, with the energy gain from hybridization increased by decreasing the distance. Hybridization of the corresponding Op and and Bd orbitals leads to a bonding and an antibonding "molecular" orbital, as depicted in Fig. 10b). If the d shell of the B ion is empty, the two electrons from the O^{2-} ion (arrows) exactly fill the bonding orbital, maximizing the energy gain from hybridization. In contrast, any d electrons from B would have to go into the anti-bonding orbital, lowering the energy gained.

While the above consideration makes plausible the strong preference for Bd^0 configurations for this "traditional mechanism of ferroelectricity", I should remark that it is no absolute theorem and additional factors likely participate, but the detailed discussion we have to omit here [25]. In any case, the connection between the "traditional mechanism of FE" in perovskites and the "d^0th-ness" of the B ion is established empirically.

The challenge, then, is to combine magnetism and FE despite the above-mentioned incompatibility. The conceptually simplest approach is to fabricate multi-phase materials or thin film hetero-structures, using $BaTiO_3$ or another traditional FE and a magnetic and magnetostrictive material such as $CoFe_2O_4$. Before briefly discussing this approach in subsection 3.5, we will focus on single-phase multiferroics (in the wider sense of magnetically and electrically ordered materials). The focus here will be on the experimental side; for a review of different approaches focusing on theory see [26].

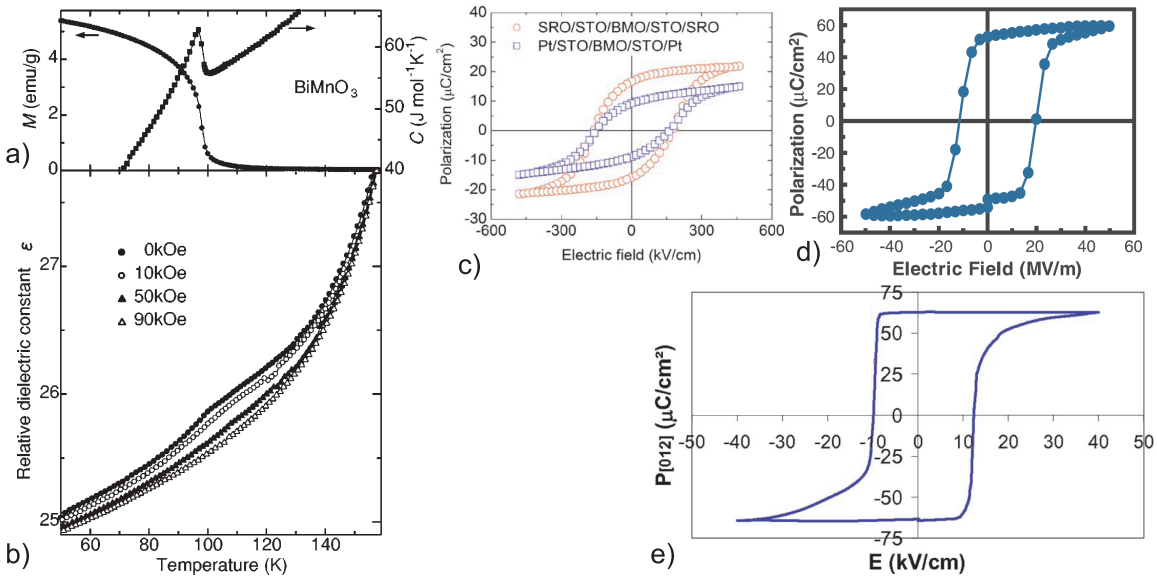

Fig. 12: *a) $BiMnO_3$ specific heat and low-field magnetization [30]. b) $BiMnO_3$ dielectric constants in different magnetic fields [30]. c) $BiMnO_3$ Polarization [31]. d/e) $BiFeO_3$ thin film [32]/single crystal [33] polarization.*

The straight-forward way to achieve both magnetism and FE in a single structure is for the former to to originate from one subunit or ion, and the latter from another. For perovskites, one can for example on the B site partially substitute a ferroelectrically active (d^0) ion with a magnetic ion. The general main problem with such an approach is that due to the different ions (or subunits) involved in magnetism and FE, the magnetoelectric coupling tends to be very low in most cases [28].

As a concrete example of the "independent subsystems" approach we consider FE due to lone pairs at the A site in perovskites with magnetic B ions [29]. Lone pairs are electrons not used in chemical bonds, occurring for example in water molecules as shown in Fig. 11a). Lone pairs are highly polarizable, contributing e.g. to the polarizability of water. In perovskites, A site Bi^{3+} or Pb^{2+} have $6s$ electrons not participating in bonds and thus yielding lone pairs, see Fig. 11b). If these lone pairs are localized and ordered in one direction, inversion symmetry is broken and an electric polarization results. In $PbTiO_3$ this lone-pair mechanism helps the traditional mechanism stabilizing the FE.

In $BiMnO_3$, the B site Mn^{3+} ions lead to FM below $100\,\mathrm{K}$ (see Fig. 12a). The Bi lone pairs alone are sufficient to also stabilize FE (below $800\,\mathrm{K}$), as indicated by polarization hysteresis loops (Fig. 12c). The occurrence of both *ferro*electricity and *ferro*magnetism make this an exceptional example of a real multiferroic in the strictest definition [34]. Despite of this, however, the magnetoelectric coupling is very weak, as indicated by an only very small (and almost magnetic-field-independent) feature in the dielectric constant at the magnetic ordering temperature (Fig. 12b) [30]. The smallness of the dielectric feature at the magnetic transition is consistent with the expectation for an "independent subsystem" multiferroic.

In $BiFeO_3$ [35], the Fe spins order antiferromagnetically below $643\,\mathrm{K}$, in a complex spin structure based on G-type antiferromagnetism (i.e. with each Fe ion surrounded by six antiparallel nearest neighbors) [36]. Bi lone pairs again lead to FE, below $1100\,\mathrm{K}$, with polarization hysteresis loops both on thin films and more recently on high-quality single crystals (panels d,e) showing the intrinsic nature of a high ($> 60\,\mu\mathrm{C/cm^2}$, comparable with $BaTiO_3$) polarization at

room temperature [32, 33]. Room-temperature MF would make $BiFeO_3$ a very good prospect for applications if a significant magnetoelectric coupling were present as well. In analogy with $BiMnO_3$, we would expect only very small coupling. However, sizeable coupling and control of magnetism by electric fields has been demonstrated experimentally. The origin of this is connected with a spiral part of the magnetic structure and corresponding couplings in the class of "spiral multiferroics". I will therefore return to this issue later.

There are many more examples of "independent subsystem" multiferroics, which typically have FE transitions at much higher temperature than the magnetic transitions, and can have sizeable electric polarization [28]. The main challenge in this group of materials is to achieve (and understand) a significant magnetoelectric coupling.

3.3 Ferroelectricity from Spin-Spirals

In the next class of multiferroics to be considered [39, 40], the situation is reversed. These materials have FE transitions at the same or, more typically, lower temperatures as the magnetic transitions, typically show large magnetoelectric couplings as observed by magnetic-field effects on dielectric constants and polarization, but conversely have much smaller electric polarizations.

The first [37], and possibly most, studied example of this class is $TbMnO_3$, which also crystallizes in a perovskite-type structure (c.f. Fig. 10a), with Tb at the A and Mn at the B site (similar effects also occur when Tb is replaced by other rare earths, e.g. Dy or Gd). The Mn spins order around $40\,\mathrm{K}$, with an additional magnetic phase transition at $26\,\mathrm{K}$. Additionally, Tb $4f$ moment order appears below $10\,\mathrm{K}$. The magnetic transitions are well visible in magnetization and specific heat data (Fig. 13a). An electric polarization in c direction appears at the $26\,\mathrm{K}$ magnetic transition (Fig. 13b), already an indication of a "magnetically driven" FE. The value of the polarization, $800\,\mu\mathrm{C/m^2} = 0.08\,\mu\mathrm{C/cm^2}$ is very small compared to traditional FE, with typical values $> 10\,\mu\mathrm{C/cm^2}$, or also some of the MF discussed above.

By the application of a magnetic field $\|b$ the direction of the polarization can be changed from c to a (Fig. 13c/d), evidence of an enormous electromagnetic coupling [37]. The polarization flop correlates with a meta-magnetic transition, and a detailed understanding of the magnetic structure in the different phases seems to be required to address this issue, as well as the general origin of the FE in $TbMnO_3$ and related compounds. Neutron and resonant x-ray diffraction

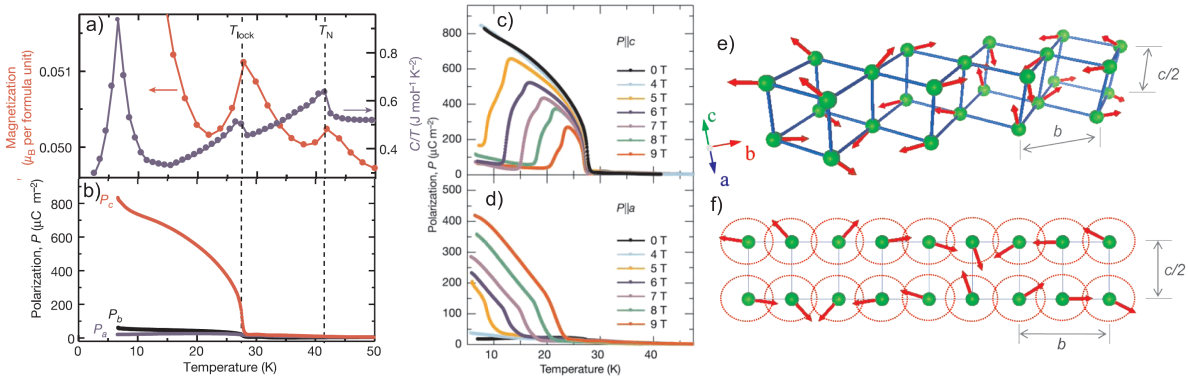

Fig. 13: *$TbMnO_3$ a/b) T dependence of magnetization, specific heat, and electric polarization. c/d) c and a component of polarization in different magnetic fields applied $\|b$. Panels a-d after [37]. e/f) Spin structure below $26\,\mathrm{K}$, with projection to bc plane [38].*

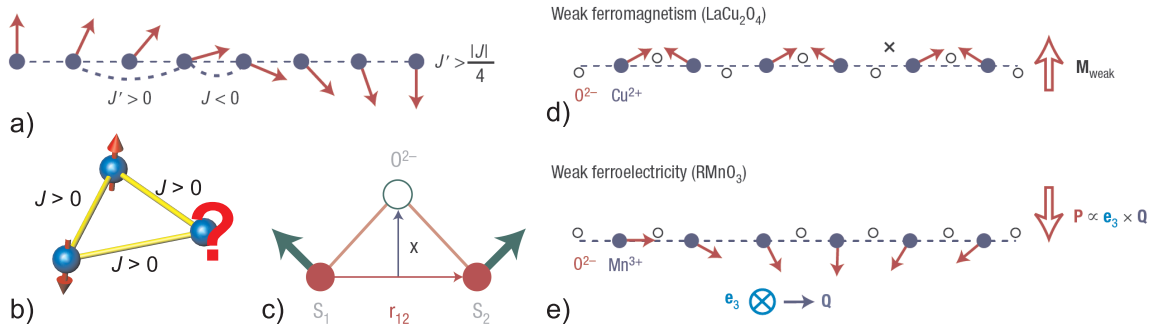

Fig. 14: *a) Spiral (cycloidal) spin order arises as classical ground state of Heisenberg spin chain with nearest neighbor FM and next-nearest neighbor AFM coupling. b) Frustration of Ising spins with AFM nearest-neighbor coupling on a triangle. c) Illustration of Dzyaloshinskii-Moriya interaction interaction (DMI) between two magnetic ions (see text). d) DMI can lead to weak ferromagnetism in antiferromagnets such as Fe_2O_3 or $LaCu_2O_4$. e) DMI can also lead to weak ferroelectricity in spiral magnets. Panels a and c-e after [39].*

data indicate that the spins initially order in an incommensurate, but almost collinear (slightly canted) amplitude-modulated structure [41, 42, 43]. The 26 K transition corresponds to the transformation into a spiral (cycloidal) spin structure, shown in Fig. 13e/f). The spins rotate around the a axis, whereas the propagation is along b. This specific spin configuration seems to be connected with a polarization along c.

The absence of an electric polarization associated with the high T spin structure and both the presence and the direction of the polarization in the low T cycloidal spin structure can be understood from symmetry-arguments on a phenomenological level [44]. While any spin ordering breaks time-reversal symmetry, an electric polarization also needs broken inversion symmetry (Fig. 7a). The spin structure above 26 K is inversion-symmetric, and therefore cannot give rise to any polarization. The cycloidal low T structure, on the other hand, is not inversion-symmetric (spatial inversion inverts the sense of direction of the rotation of the spins), allowing for an electric polarization. This is formalized using a Ginzburg-Landau free energy density approach, which in the simplest case of cubic symmetry gives a polarization [44]

$$\vec{P}(\vec{r}) = \gamma\chi_e \left[\left(\vec{M}(\vec{r}) \cdot \nabla \right) \vec{M}(\vec{r}) - \vec{M}(\vec{r}) \left(\nabla \cdot \vec{M}(\vec{r}) \right) \right], \tag{1}$$

where χ_e is the electric susceptibility. This symmetry argument shows that electric polarization can arise from spatially inhomogeneous non-centrosymmetric magnetism.

The mechanism by which such magnetic structures arise is "frustration", the existence of competing interactions. Consider for example a Heisenberg Spin chain (Fig. 14a): with only nearest-neighbor interaction $J\vec{S}_n \cdot \vec{S}_{n+1}$ the ground state is either a parallel ($J < 0$) or alternating ($J > 0$) spin-arrangement, but if there is a FM nearest-neighbor coupling $J < 0$ and a sufficiently strong AFM next-nearest-neighbor coupling $J' > -J/4$ the ground-state is a cycloid, as realized in $TbMnO_3$. Frustration and correspondingly complex spin configurations can also arise with only nearest-neighbor interactions, for example on triangular lattices with AFM coupling (Fig. 14b). Returning to the cycloid, it can be described by

$$\vec{S}(\vec{r}_n) = S_1 \vec{e}_1 cos(\vec{q} \cdot \vec{r}_n) + S_2 \vec{e}_2 cos(\vec{q} \cdot \vec{r}_n), \tag{2}$$

where the unit vectors $\vec{e}_i$, $i = 1, 2, 3$ form an orthonormal basis, $\vec{e}_3$ being the direction around which the spins rotate, and $\vec{q}$ is the propagation vector. The cycloidal ground state has $S_1 = S_2$,

$\overrightarrow{q} \perp \overrightarrow{e}_3$, and $|\overrightarrow{q}| = 2\arccos(-J'/4J)$. The spins S_i provide the magnetization M_i, and the average polarization is then obtained with Eq. (1) as

$$\langle \overrightarrow{P} \rangle = V^{-1} \int \overrightarrow{P}(\overrightarrow{r}) d^3r = \gamma \chi_e M_1 M_2 [\overrightarrow{e}_3 \times \overrightarrow{q}]. \tag{3}$$

Eq. (2) can describe also states other than a cycloidal. For example, for $\overrightarrow{q} \| \overrightarrow{e}_3$ it describes a proper screw instead: it is clear from Eq. (3) that there is no uniform polarization in this case. Also, the pure sinusoidal amplitude modulation that due to magnetic anisotropies has to replace the cycloidal ground state at sufficiently high T, as is the case in $TbMnO_3$, is described by Eq. (2), by simply setting either S_1 or S_2 to 0. Again, there is no average polarization according to Eq. (3) − consistent with the experiment. Finally, the "polarization" flop upon application of a magnetic field (Fig. 13c/d) is associated with a flop in the cycloidal spin-rotation axis, further confirming the model [45].

Intense research activity in the past few years has uncovered countless examples of materials with FE associated with spin spirals [28]. These materials have very diverse crystal structures, but Eq. (3), despite being a simplification neglecting e.g. anisotropy effects, holds in most cases. However, this phenomenological description does not address the microscopic origin of spin-spiral-based FE and in particular can not provide any estimate of the magnitude of the polarization that may be expected. A plausible microscopic mechanism [46] that at least contributes to the spin-spiral FE is the ion displacement due to the antisymmetric Dzyaloshinskii-Moriya (DM) interaction [47], which is a relativistic correction to the usual superexchange $J \overrightarrow{S}_i \cdot \overrightarrow{S}_j$. It is described by an energy term of the form

$$E_{ij}^{DM} = \overrightarrow{D}_{ij} \cdot \left(\overrightarrow{S}_i \times \overrightarrow{S}_j \right), \tag{4}$$

where $\overrightarrow{D}_{ij}$ is a material-specific vector-coefficient. For superexchange between two neighboring magnetic ions via oxygen as depicted in Fig. 14c), $\overrightarrow{D}_{ij} \| \overrightarrow{x} \propto \overrightarrow{r}_{12}$, further D_{ij} is also proportional to the spin-orbit coupling constant. As such, $|\overrightarrow{D}_{ij}|$ is a measure of local inversion-symmetry breaking, and the interaction absent when there is a center of inversion between the two magnetic ions. Discovered around 1960 [47], the DM interaction was first used to explain the weak FM observed in some primarily AFM crystals of low symmetry, such as common rust Fe_2O_3, or $LaCu_2O_4$. The situation in the latter material is sketched in Fig. 14d). Normal symmetric superexchange leads to AFM order with alternating horizontal Cu spins. However, because the oxygen ions mediating the exchange are offset from the line connecting the Cu ions, the DM term (4) is also present. In this case, $\overrightarrow{D}_{ij}$ has alternating sign, and minimization of the energy is obtained by a small canting of the spins with correspondingly alternating $\overrightarrow{S}_i \times \overrightarrow{S}_j$, yielding a net magnetic moment perpendicular to the spin chain [39].

For the spin-spiral, the reverse occurs (Fig. 14e). Here, the spin-canting is the starting point, and $\overrightarrow{S}_i \times \overrightarrow{S}_j$ has the same sign for all pairs of neighboring magnetic sites. Correspondingly, the energy can be lowered by creation of $\overrightarrow{D}_{ij}$ by displacing the oxygen ions all in the same direction perpendicular to the chain ($\overrightarrow{q}$) and the spin-rotation axis. Therefore, this "inverse DM" model predicts the same direction of the polarization as the phenomenological Eq. (3). It should be remarked that in addition to these ion displacement considerations there is also a purely electronic contribution [48]. However, comprehensive density functional calculations suggest that the ionic contribution to the FE polarization is dominant, at least in $TbMnO_3$ [49, 50]. As a microscopic model, the strength of the coupling D_{ij} and the resulting polarization can

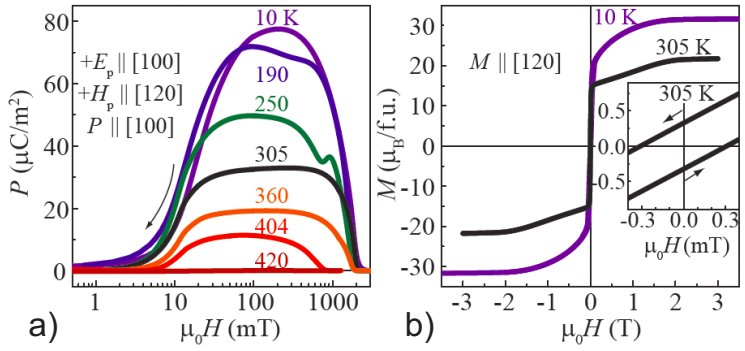

Fig. 15: *Room-temperature multiferroicity in the Z-type hexaferrite $(Ba_{0.17}Sr_{0.83})_3Co_2Fe_{24}O_{41}$ induced by magnetic fields H. a) Electric polarization P vs H at different T. b) Magnetization vs H. After [51].*

be calculated. Unfortunately, the coupling strength is set by the spin-orbit coupling, which as a relativistic effect is intrinsically very small. Correspondingly, the small polarization measured on $TbMnO_3$ is not a coincidence, but rather polarizations reaching more than $1\,\mu C/cm^2$ cannot be expected for spin-spiral based FE, values that may be too low for many applications.
Another problem with respect to potential applications until recently was the very low temperature scale, e.g. 26 K by $TbMnO_3$ (Fig. 13a), rather typical for spin-spiral FE. The basic reason for this is that the frustration inherently needed for the creation of the spin spiral also suppresses the ordering temperature. However, in recent years, spin-spiral FE with temperature scales reaching room temperature were discovered, most prominently the large family of hexaferrites with several complex structure types. Here, proper-screw type magnetic structures transform into transverse-conical spin structures upon application of a small magnetic field (see, e.g., [52]). In the hexaferrite $Ba_{0.17}Sr_{0.83})_3Co_2Fe_{24}O_{41}$ MF at room temperature has been unambiguously demonstrated (see Fig. 15 [53, 51]) and further exploration of the family holds promise of discovering compounds suitable for IT applications.

3.4 Collinear "magnetic ferroelectrics" and ferroelectricity from charge order

As the electric polarization of the spin-spiral FE is intrinsically limited by the weak spin-orbit coupling, the question arises whether there are any other mechanisms through which FE can be generated by magnetism. This is indeed the case, and I will describe here one mechanism and a corresponding example compound. Consider a chain of alternating ions (Fig. 16b). These may be different elements, or alternatively ions of one element in different valence states. The ions should be all magnetic with magnetic anisotropy providing an Ising-chain. If we have competing interactions as in Fig. 14a), but Ising instead of Heisenberg spins (i.e. we have uniaxial magnetic anisotropy), the ground state (for $J' > -J/2$) is an $\uparrow\uparrow\downarrow\downarrow$ configuration as indicated in Fig. 16b). As the magnetic exchange between neighboring ions depends on the distance between them, there is in the reverse also an exchange striction, which will tend to decrease the distance between neighboring ions with parallel spin-alignment. The result is pairs of ions corresponding to electric dipoles (c.f. Fig. 16b). It is remarkable that both the alternating-ion chain without the spins and the spin-chain ignoring the difference between the two ions are centrosymmetric. Inversion-symmetry is only broken, and FE allowed, by their combination. Because this mechanism does not depend on relativistic effects, much larger electric polarizations than in the spin-spiral FE might be expected [54].
A rather clear example of the above mechanism is provided by Ca_3CoMnO_6 [55], whose crystal structure provides for chains of alternating Co and Mn, and where Ising-magnetism with $\uparrow\uparrow\downarrow\downarrow$

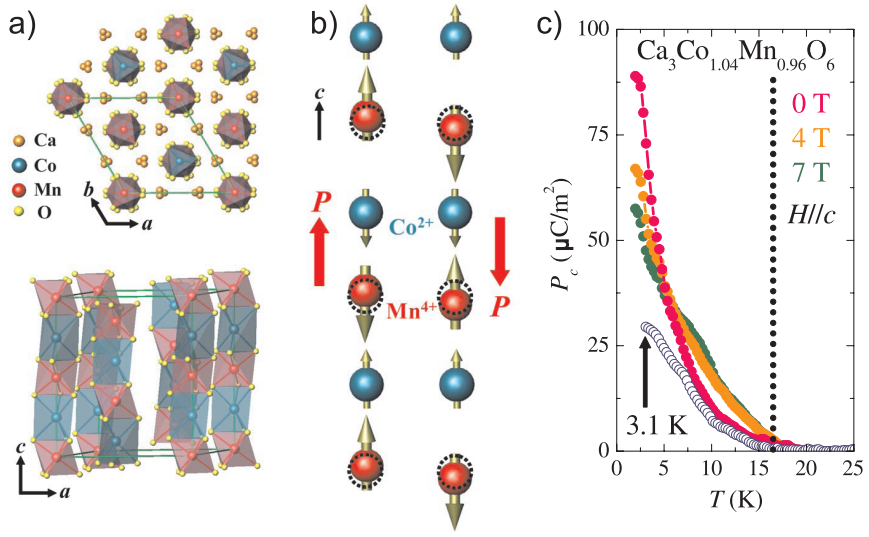

Fig. 16: *Ca_3CoMnO_6 [55]. a) Crystal structure b) Co/Mn Ising chains with two states of ↑↑↓↓ spin ordering. Ions are displaced from ideal positions (broken circles) by magnetostriction, leading to an electric polarization. c) Polarization from pyroelectric current measurements.*

spin arrangement along these chains occurs (Fig. 16a/b). As shown in Fig. 16c), pyroelectric current measurements indeed indicate a spontaneous electric polarization below the onset of magnetic order [55]. Unfortunately and contrary to the expectation, the observed polarization is even lower than in $TbMnO_3$. Likely, this exchange-striction mechanism is also the principal driving force for FE in the double-layer manganites, where however different Mn valence states provide for one of the necessary preconditions [54]. In those compounds also only small polarizations are observed.

Apart from the spin degree of freedom there are two other electronic degrees of freedom, charge and orbital. Ordering of one of these degrees of freedom may result in FE as well [54]. In particular, one can expect to obtain an electric polarization from any charge ordering (CO), the localization of charge carriers on parts of the ions in a spatially periodic fashion, that breaks spatial inversion symmetry. Although MF then is not quite as inherent as in the case of spin-based FE, the fact that the electrons that are involved in charge or orbital order inevitably also have uncompensated spins provides for a high probability of multiferroicity to result. Furthermore, because the same electrons are involved in the different orderings, a significant coupling can be expected as well. The main advantage of FE from CO, compared to "magnetic ferroelectricity", is that much higher electric polarizations can be expected.

The difficulty in obtaining FE from CO is that the Coulomb-interaction driving the CO tends to avoid non-centrosymmetric configurations. An example of how a non-centrosymmetric and thus ferroelectric CO could be obtained is given by considering charge order on a chain [54]. If there is one electron per two sites, the expectation is to obtain a chain with ions of alternating valence states. However, apart from this situation, termed "site-centered" charge order, it is also possible that the electrons localize on the bonds between the ions in a "bond-centered" charge order, a situation realized by a Peierls-distortion well-known in low-dimensional (mainly organic) compounds. Here, the ions remain equivalent, but not the bonds between them, and, as a result, there is a tendency to dimerization. Neither "site-centered" nor "bond-centered" charge order breaks inversion-symmetry by itself, but their combination does [56, 54]. The situation and resulting electric dipoles is the same as in Fig. 16b), except that the ion shifts are due to "bond-centered" charge order rather than magnetostriction (and the coloring is due to "site-centered" charge order). Such a mechanism was proposed to be active [56] in Ca-doped $PrMnO_3$ for certain intermediate Ca doping, but direct experimental confirmation of this scenario has not been obtained, not least due to a too large conductivity of (Pr,Ca)MnO_3.

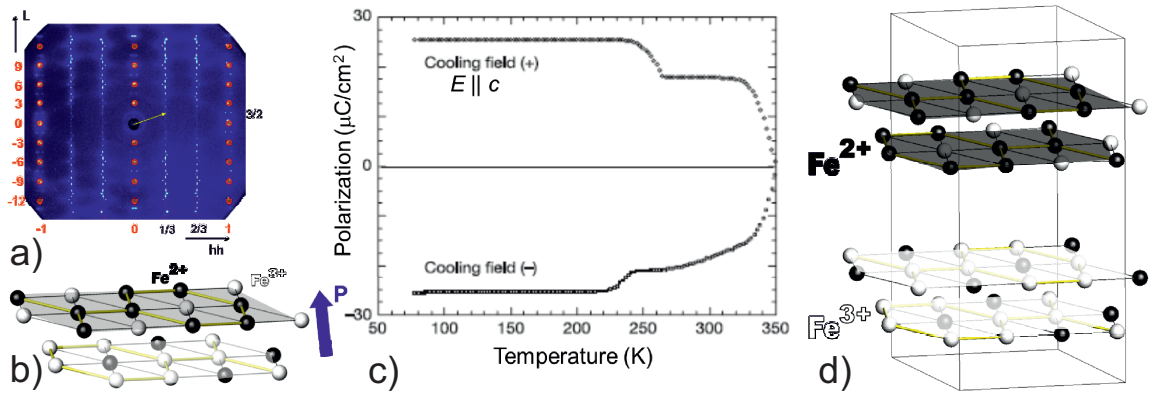

Fig. 17: *Ferroelectric charge order CO in $LuFe_2O_4$? a) CO reflections by high-energy x-ray diffraction. b) Model, proposed in 2005 [57], of the $Fe^{2+/3+}$ CO in Fe/O bilayers, the basic structural subunit. Different average valence of the two layers makes the bilayer polar, indicated by the arrow. c) Pyroelectric current measurements [57] indicated a large ferroelectric polarization. d) Recently revised model of the CO, based on the first structure refinements [58]: The bilayers are charged rather than polar, excluding ferroelectricity due to CO.*

Unambiguous confirmation of FE due to CO is elusive also in other compounds so far, and there are as yet only few examples, none of them absolutely clear. We first discuss an example that scattering methods recently showed is rather a non-example: The material most often cited as the prototypical example of CO-based FE (see, e.g., [28]) is $LuFe_2O_4$, which has a layered crystal structure with Fe/O bilayers as the the electronically active subunit. The Fe ions have an average valence of $2.5+$, so a Fe^{2+}/Fe^{3+} charge ordering can be expected. Superstructure reflections that can be attributed to charge order do indeed appear slightly above room temperature (Fig. 17a). The location of these reflections at "$(h, h) = (\frac{1}{3}, \frac{1}{3})$" and equivalent is consistent with the charge configuration within a bilayer indicated in Fig. 17b), first proposed by Ikeda and coworkers in 2005 [57]. Because one of the two layers is rich in Fe^{2+} and the other in Fe^{3+} (as indicated by a shading of the layers), the bilayer would become polar by such a CO. In accordance with this polar CO model, pyroelectric current measurements (Fig. 17c) suggested a spontaneous polarization, also up to slightly above room temperature [57]. Although these polar bilayers were generally accepted in the extensive literature on $LuFe_2O_4$, a direct proof for or against was lacking. Only very recently, the charge-ordered crystal structure could be refined based on single-crystal x-ray diffraction data measured on an almost-mono-domain crystal. The Fe^{2+}/Fe^{3+} arrangement deduced from the refinement, which is supported also by x-ray magnetic circular dichroism and neutron diffraction, contains bilayers that are charged rather than polar (Fig. 17d), excluding CO-based FE in $LuFe_2O_4$ [58].

A remarkable, *if verified*, example of CO-driven FE would be classical magnetite Fe_3O_4, the oldest magnetic material known to mankind and also the classical (1939) example of a CO transition. Despite decades of research, the very complex CO structure of magnetite has eluded a determination until recently, when Senn and coworkers achieved a refinement based on high-energy x-ray diffraction on a tiny ($40\,\mu$m) almost-mono-domain crystal [59]. The refined structure, consistent with density-functional calculations [60] is indeed polar, which leaves only to show that it can actually be switched by an electric field. The latter is complicated by residual conductivity and associated "relaxor-like characteristics", indicated by dielectric spectroscopy [61].

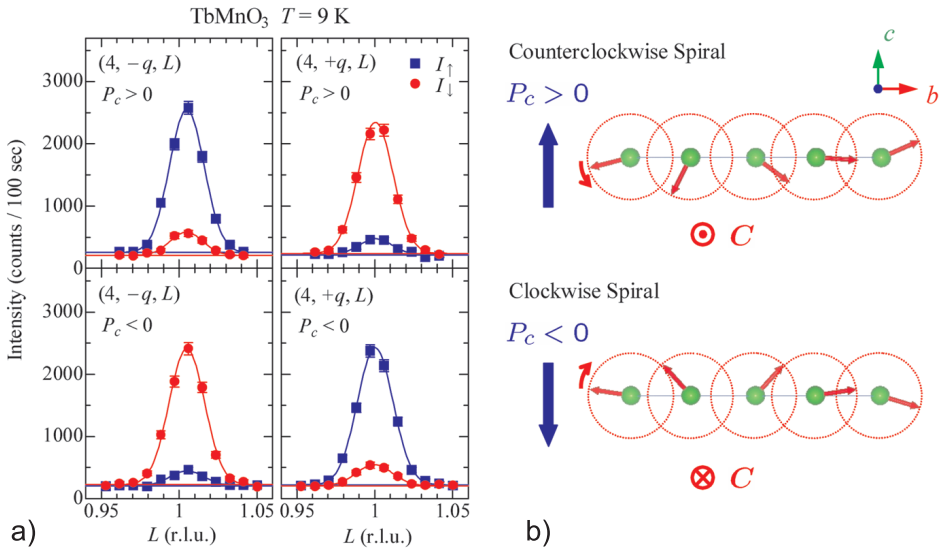

Fig. 18: *Electric-Field control of magnetic state in $TbMnO_3$ [38]. a) Polarized neutron scattering dependence on Polarization, selected by voltage bias on cooling. b) correspondence of spin-spiral helicity and polarization.*

3.5 Electric-field control of magnetism and multiferroic heterostructures

Indications for magnetoelectric coupling have been observed for many MF within the different "classes" described above. For the spin-spiral FE in particular, control of the electric polarization by a magnetic field has been shown in a dramatic way already in the first paper [37] (Fig. 13c/d). Given the mechanism by which the polarization arises directly from the spin structure, this is hardly surprising. However, for many applications such as the MF-RAM (Fig. 9) it is more important to control the magnetization by an electric field. Demonstrations of magnetoelectric coupling in this direction are much more rare. Still, the DM interaction as an energy contribution Eqn. (4) works both ways, as we have seen also from the example of weak FM.

In the spin-spiral FE there is generally no spontaneous magnetization that can be switched, but on the other hand reversing the sense of rotation along the spiral reverses the associated FE polarization (Fig. 18b), therefore switching the polarization by an applied electric field should be able to revert the sense of rotation of the spins. The technique most suited to measure the sense of rotation is polarized neutron scattering, because the intensity of magnetic reflections will be different for the neutron spins parallel or antiparallel to the chirality of the spin-spiral. Measurements on $TbMnO_3$ (Fig. 18a) indeed showed different sense of rotations of the spins after cooling to the FE phase in a positive or negative electric field [38].

Whereas strong magnetoelectric coupling is inherent in the spin-spiral FE, this is not the case for MF in general, as we have seen on the example of $BiMnO_3$. Surprisingly, electric-field control of magnetism is possible in $BiFeO_3$ [62], despite of this material being in the same "class" of MF as $BiMnO_3$. To understand why, we need to consider the magnetic structure [36]: it is based on a G-type AFM, where each Fe site spin has six antiparallel nearest neighbors, but overlaid on this are a spin-canting and long-period cycloidal modulation (Fig. 19b). The cycloidal modulation in this case does not arise from magnetic frustration, but rather is a consequence of the DM interaction (4). Indeed, it was long known that apart from creating weak FM, the DM interaction can also lead to cycloidal spin configurations. The mechanism is exactly as discussed above and sketched in Fig. 14e), except that the off-centering of the oxygen ions is the origin rather than the effect. In $BiFeO_3$, this off-centering is due to the electric polarization, which in turn is driven by the "lone-pair" mechanism. This compound is therefore the opposite to $TbMnO_3$: rather than FE due to spin-spiral, we have spin-spiral due to FE. Different direc-

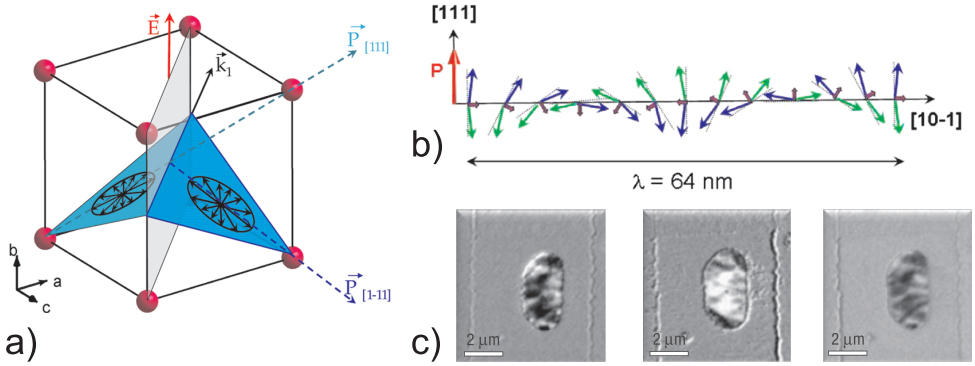

Fig. 19: *Electric-Field control of magnetic state in $BiFeO_3$. a) sketch of spiral domains and relation-ship with polarization [62]. Domains can be selected by external electric field. b) in one domain, spin structure is given by superposition of G-type antiferromagnetic order, spin canting, and long-period spiral [62]. c) XMCD-PEEM images [63] showing magnetic contrast of a CoFe-layer, whose magnetization is switched using exchange-bias to an adjacent $BiFeO_3$ layer, the magnetism of which is controlled by an electric field. Images left to right are obtained by two consecutive electrical field switches.*

tions of the polarization will correspond to different possible directions (domains) of the spin spiral (Fig. 19a), providing a mechanism for switching of magnetic domains by an electric field, as demonstrated by Lebeugle and coworkers [62].

Because all this works even at room temperature, $BiFeO_3$ appears to be a most promising candidate for building MF-RAM cells (Fig. 9) and similar applications. What is needed next is a mechanism, such as exchange bias (see lecture E5), through which the magnetic domain configuration of $BiFeO_3$ is linked to the ferromagnetic domain structure of an adjacent soft FM. This was successfully demonstrated by Chu and co-workers [63], who built a heterostructure with $BiFeO_3$ and CoFe as the soft FM (see also [64]. In Fig. 19c) three XMCD-PEEM images of this device, with a small CoFe island in the center, are shown. The contrast is given by different magnetic polarities. Between neighboring images, an electric field is applied, first in one, then in the other direction. The clearly visible switching of the CoFe magnetization by the electric field was achieved at room temperature.

In multiferroic devices such as the MF-RAM (Fig. 9) the materials occur not in the bulk form, but in (patterned) heterostructures. In this case interface effects can be of crucial importance. A good example is the use of the exchange-bias effect between a FM and an AFM FE, e.g. for a CoFe-$BiFeO_3$ heterostructure as discussed just above (c.f. Fig. 19c). But with interface effects it is even possible to create composite multiferroics out of materials that are all non-multiferroic intrinsically. One approach (for reviews see, e.g., [65, 66]) uses strain at the interface to couple a FE material (via the piezoelectric effect) to a FM material (via magnetostriction). This works best with FE with large piezoelectric coefficents (in particular $Pb(Zr,Ti)O_3$ or PZT) and FM with large magnetostriction. In such systems, magnetoelectric coupling coefficients more than two orders of magnitude larger than in single-phase MF have been observed. However, while the concept of strain-coupling is simple, the detailed modeling is difficult, and so is experimental reproducibility, given strong influence of defects, domains etc.

A more recent approach uses the strong sensitivity of correlated oxides to charge carrier density, employing FE gate oxides. The two polarization states of the gate, tunable by low voltages, then correspond to two different effective doping levels in the magnetically active correlated oxide.

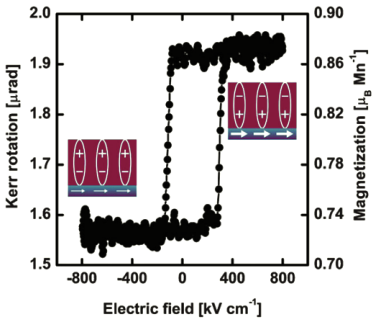

Fig. 20: *Magnetoelectric hysteresis-loop showing the magnetic response (Kerr-rotation $\propto$ M) as a function of applied electric field at* $100\,\mathrm{K}$ *of a PZT(*$250\,\mathrm{nm}$*)-*$La_{0.8}Sr_{0.2}MnO_3$*(*$4\,\mathrm{nm}$*) heterostructure grown on a* $SrTiO_3$*(001) substrate. Insets represent the magnetic and electric states of the two layers. After [67].*

For the latter, doped perovskite manganites, such as $La_{1-x}Sr_xMnO_3$, which are characterized by competing phases and an intricate interplay of magnetism, structure, and electron transport [68], can be employed. For an appropriate composition, the additional effective doping by the gate can trigger a transition to a phase with different magnetic properties. Following this recipe, Molegraaf and coworkers [67] have recently demonstrated a large magnetoelectric coupling in a PZT-$La_{0.8}Sr_{0.2}MnO_3$ bilayer heterostructure (Fig. 20). The effect shown is much larger than in single-phase multiferroics and approaches values of strain-coupled multiferroic heterostructures, while being of purely electronic origin [69]. Similarly, an electronic reconstruction at the interface between a FM and a FE can induce a purely magnetoelectric coupling, as recently demonstrated for $BaTiO_3$ and Fe or Co [70].
For the realization of an MF-RAM (Fig. 9) and further spintronic applications it is also necessary to consider the transport properties of multiferroic heterostructures, i.e. multiferroic tunnel-junctions. Such a tunnel junction depending both on electric and magnetic states for a total of four memory states has already been demonstrated [71]. There is currently much research being conducted in this field closest to application, and promising results can be expected.

4 Concluding remarks

On the way towards non-volatile memory applications actually on the market, phase change materials are further advanced than multiferroics. In fact, a 512 Mbit PC-RAM is already used as a replacement of slower flash in some mobile phones [72]. However, the relatively low storage capacity compared to the currently available 64 Gbit flash-based USB sticks suggests scalability problems and additionally the high operating current densities force device architectures that put the PC-RAM to a severe cost-disadvantage compared to Flash. These problems will have to be overcome if PC-RAM is to become more than a niche product. Aiming towards an universal memory (Sec. 1), new routes need to be pursued in research. One such route, going from single phases to heterostructures, is starting to be pursued, with promising results [73]: in a multilayer $(GeTe)_2$-$(Sb_2Te_3)_4$ system, switching currents considerably lower and lifetimes orders of magnitude higher than for $Ge_2Sb_2Te_5$ have been observed.
For multiferroics, on the other hand, the room-temperature switchability of a magnetic layer, crucial for the MF-RAM, has been shown using $BiFeO_3$ [63, 64], and also on heterostructures such as Pb(Zr,Ti)O_3-$La_{0.8}Sr_{0.2}MnO_3$ [67], though the issue of the (presumably fast) time scales of the switching have to be addressed experimentally. However, so far a fully functioning MF memory cell has yet to be demonstrated, and from there to an integrated circuit it is still a way to go. All this suggests that it will still be some time before we can expect to buy devices that use MF-RAM. A large contrast to the PCM with their rather common mechanism

and clear location on a "treasure map" (Fig. 5a) is that there are many potential ways towards multiferroicity. Currently rather classical $BiFeO_3$ with its lone-pair ferroelectricity seems to have the lead, but good progress is also being made recently with spin-spiral based ferroelectrics such as hexaferrites, and artificial heterostructures show promise as well. This richness of materials, effects, and mechanisms in multiferroics provides for some unpredictability, but also for chances in the medium and long term. Of course, in the long term, some of the various more exotic concepts mentioned in Sec. 1, that could not be covered in detail, might prevail.
In any case, research on a materials or heterostructure level, will continue for both PCM and multiferroics to contribute critically to the eventual realization of integrated devices. I hope that this lecture also showed how the application of a large variety of scattering methods is crucial to make progress in understanding these PCM and multiferroics. Although the scattering examples shown are all from bulk systems, I would like to stress that scattering methods are also indispensable for the detailed understanding of heterostructures, the last step short of a device.

Acknowledgment

I gratefully acknowledge R. P. Hermann for contributing graphics used in Sec. 2, and A. Weber for proof-reading of the lecture notes.

References

[1] D. Loss and D. P. DiVincenzo, Phys. Rev. A **57**, 120 (1998).

[2] L. DiCarlo *et al.*, Nature **460**, 240 (2009).

[3] F. Schwierz, Nat. Nanotech. **5**, 487 (2010).

[4] R. Waser, R. Dittmann, G. Staikov, and K. Szot, Adv. Mater. **21**, 2632 (2009).

[5] L. Bogani and W. Wernsdorfer, Nat. Mater. **7**, 179 (2008).

[6] P. Fromherz, A. Offenhausser, T. Vetter, and J. Weis, Science **252**, 1290 (1991).

[7] M. Wuttig and N. Yamada, Nat. Mater. **6**, 824 (2007).

[8] I. Friedrich, V. Weidenhof, S. Lenk, and M. Wuttig, Thin Solid Films **389**, 239 (2001).

[9] W. Welnic and M. Wuttig, Materials Today **11**, 20 (2008).

[10] N. Yamada *et al.*, J. Appl. Phys. **69**, 2849 (1991).

[11] G. Atwood, Science **321**, 210 (2008).

[12] S. R. Ovshinsky, Phys. Rev. Lett. **21**, 1450 (1968).

[13] C. Kim *et al.*, Appl. Phys. Lett. **94**, 193504 (2009).

[14] K. Shportko *et al.*, Nat. Mater. **7**, 653 (2008).

[15] L. Pauling, *Nature of Chemical Bond* (Cornell Univ. Press, New York, 1939).

[16] D. Lencer *et al.*, Nat. Mater. **7**, 972 (2008).

[17] S. Kohara *et al.*, Appl. Phys. Lett. **89**, 201910 (2006).

[18] J. Hegedus and S. R. Elliott, Nat. Mater. **7**, 399 (2008).

[19] T. Matsunaga *et al.*, Adv. Funct. Mat. **21**, 2232 (2011).

[20] H. Schmid, Ferroelectrics **162**, 317 (1994).

[21] N. A. Spaldin, M. Fiebig, and M. Mostovoy, J. Phys.: Condens. Matter **20**, 434203 (2008).

[22] M. Bibes and A. Barthélémy, Nat. Mater. **7**, 425 (2008).

[23] J. Nogués and I. K. Schuller, J. Magn.Magn. Mater. **192**, 203 (1999).

[24] N. A. Hill, J. Phys. Chem. B **104**, 6694 (2000).

[25] D. I. Khomskii, J. Magn. Magn. Mater. **306**, 1 (2006).

[26] S. Piccozzi and C. Ederer, J. Phys.: Condens. Matter **21**, 303201 (2009).

[27] D. I. Khomskii, Physics **2**, 20 (2009).

[28] K. F. Wang, J.-M. Liu, and Z. F. Ren, Adv. Physics **58**, 321 (2009).

[29] R. Seshadri and N. A. Hill, Chem. Mater. **13**, 2892 (2001).

[30] T. Kimura *et al.*, Phys. Rev. B **67**, 180401(R) (2003).

[31] J. Y. Son and Y.-H. Shin, Appl. Phys. Lett. **93**, 062902 (2008).

[32] J. Wang *et al.*, Science **299**, 1719 (2003).

[33] D. Lebeugle, D. Colson, A. Forget, and M. Viret, Appl. Phys. Lett. **91**, 022907 (2007).

[34] Note that ferroelectricity in ideal stoichiometric $BiMnO_3$ has recently become a very controversial issue, with antiferroelectricity as an alternative. For a summary of different evidences see I. V. Solovyev and Z. V. Pchelkina, New J. Phys. **10**, 073021 (2008).

[35] G. Catalan and J. F. Scott, Adv. Mater. **21**, 2463 (2009).

[36] I. Sosnowska, T. Peterlin-Neumaier, and E. Steichle, J. Phys. C:Solid State Phys. **15**, 4835 (1982).

[37] T. Kimura *et al.*, Nature **426**, 55 (2003).

[38] Y. Yamasaki *et al.*, Phys. Rev. Lett. **98**, 147204 (2007).

[39] S.-W. Cheong and M. Mostovoy, Nat. Mater. **6**, 13 (2007).

[40] Y. Tokura and S. Seki, Adv. Mater. **21**, 1 (2009).

[41] M. Kenzelmann *et al.*, Phys. Rev. Lett. **95**, 087206 (2005).

[42] J. Voigt *et al.*, Phys. Rev. B **76**, 104431 (2007).

[43] S. B. Wilkins *et al.*, Phys. Rev. Lett. **103**, 207602 (2009).

[44] M. Mostovoy, Phys. Rev. Lett. **96**, 067601 (2006).

[45] N. Aliouane *et al.*, Phys. Rev. Lett. **102**, 207205 (2009).

[46] I. A. Sergienko and E. Dagotto, Phys. Rev. B **73**, 094434 (2006).

[47] I. Dzyaloshinsky, J. Phys. Chem. Solids bf 4, 241 (1958); T. Moriya, Phys. Rev. **120**, 91 (1960).

[48] H. Katsura, N. Nagaosa, and A. Balatsky, Phys. Rev. Lett. **95**, 057205 (2005).

[49] H. J. Xiang, S.-H. Wei, M.-H. Whangbo, and J. L. D. Silva, Phys. Rev. Lett. **101**, 037209 (2008).

[50] A. Malashevich and D. Vanderbilt, Phys. Rev. Lett. **101**, 037210 (2008).

[51] S. H. Chun *et al.*, arXiv:1111.4525.

[52] M. Soda *et al.*, Phys. Rev. L **106**, 087201 (2011).

[53] Y. Kitagawa *et al.*, Nat. Mat **9**, 797 (2010).

[54] J. van den Brink and D. I. Khomskii, J. Phys.: Condens. Matter **20**, 434217 (2008).

[55] Y. J. Choi *et al.*, Phys. Rev. Lett. **100**, 047601 (2008).

[56] D. V. Efremov, J. Van den Brink, and D. I. Khomskii, Nat. Mater. **3**, 853 (2004).

[57] N. Ikeda *et al.*, Nature **436**, 1136 (2005).

[58] J de Groot *et al.*, arXiv:1112.0978v1.

[59] M. S. Senn, J. P. Wright, and J. P. Attfield, Nature **481**, 173 (2012).

[60] K. Yamauchi, T. Tetsuya, and S. Piccozzi, Phys. Rev. B **79**, 212404 (2009).

[61] F. Schrettle *et al.*, Phys. Rev. B **83**, 195109 (2011).

[62] D. Lebeugle *et al.*, Phys. Rev. Lett. **100**, 227602 (2008).

[63] Y.-H. Chu *et al.*, Nat. Mater. **7**, 478 (2008).

[64] J. T. Heron *et al.*, Phys. Rev. Lett. **107**, 217202 (2011).

[65] R. Ramesh and N. A. Spaldin, Nat. Mater. **6**, 21 (2007).

[66] C. A. F. Vaz, J. Hoffman, C. H. Ahn, and R. Ramesh, Adv. Mat **22**, 2900 (2010).

[67] H. J. A. Molegraaf *et al.*, Adv. Mater **21**, 3470 (2009).

[68] A. P. Ramirez, J. Phys.: Condens. Matter **9**, 8171 (1997).

[69] C. A. F. Vaz *et al.*, Phys. Rev. Le **104**, 127202 (2010).

[70] S. Valencia *et al.*, Nat. Mater. **10**, 753 (2011).

[71] M. Gajek *et al.*, Nat. Mater. **6**, 296 (2007).

[72] http://www.theregister.co.uk/2010/04/30/samsung_pram_ships/.

[73] R. E. Simpson *et al.*, Nat. Nanotech. **6**, 501 (2011).